An experimental and numerical investigation of heat transfer enhancement for graphene nanoplatelets nanofluids in turbulent flow conditions

Emad Sadeghinezhad [a], Hussein Togun [a,b], Mohammad Mehrali [c,*], Parvaneh Sadeghi Nejad [d], Sara Tahan Latibari [c], Tuqa Abdulrazzaq [e], S.N. Kazi [a,*], Hendrik Simon Cornelis Metselaar [c]

[a] Department of Mechanical Engineering, University of Malaya, 50603 Kuala Lumpur, Malaysia
[b] Department of Mechanical Engineering, University of Thi-Qar, 64001 Nassiriya, Iraq
[c] Department of Mechanical Engineering and Advanced Material Research Centre, University of Malaya, 50603 Kuala Lumpur, Malaysia
[d] Advanced Informatics School, Universiti Teknologi Malaysia (UTM), 54100 Kuala Lumpur, Malaysia
[e] Department of Mechanical and Manufacturing Engineering, Universiti Putra Malaysia (UPM), 43400 Selangor, Malaysia

ARTICLE INFO

Article history:
Received 25 June 2014
Received in revised form 1 October 2014
Accepted 2 October 2014
Available online 23 October 2014

Keywords:
Graphene nanoplatelets nanofluid
Convective heat transfer
Experimental
Numerical simulation
Turbulent flow
Thermo-physical properties

ABSTRACT

In this paper, both experimental and numerical studies have been performed on the turbulent heat transfer of the graphene nanoplatelets nanofluids in a horizontal stainless steel tube that was subjected to a uniform heat flux at its outer surface. An experimental investigation was done to evaluate the heat transfer characteristics and the pressure drop of a graphene nanoplatelet (GNP) nanofluid and in numerical study, the finite volume method with standard k–ε turbulence model is employed to solve the continuity, momentum, energy and turbulence equations in three dimensional domains. The thermal conductivity and viscosity of the GNP nanofluids at concentrations of 0.025, 0.05, 0.075, and 0.1 wt% were measured prior to the heat transfer experiments. The heat transfer and the pressure drop within the flowing base fluid (distilled water) were measured and compared with the corresponding data from the correlations and numerical study. The data were satisfied within a 5% error and 2% error for the numerical work. The effects of the nanoparticle concentration and the heat flux on the enhancement of the heat transfer turbulent flow condition are presented. The Nusselt number (Nu) of the GNP nanofluid was higher than the base fluid by approximately 3–83% and increased as the flow rate and the heat flux increased. However, the increase in the pressure drop ranged from 0.4% to 14.6%. Finally, the results reveals that the GNP nanofluids could function as a good and alternative conventional working fluid in heat transfer applications.

© 2014 Elsevier Ltd. All rights reserved.

1. Introduction

Energy transport is an integral part of a wide range of fields, including oil and gas, nuclear energy, and electrical energy. Water, oil, and ethylene glycol (EG) are used as heat transfer fluids. However, the development of heat transfer fluids with an improved thermal conductivity has become increasingly critical to the performance of energy systems [1,2]. Choi and Eastman [3] have introduced the term nanofluids, which refer to fluids that contain dispersed nano-sized particles that have a higher thermal conductivity [4]. Nanofluids improve thermo-physical properties [5], such as the thermal diffusivity and the thermal conductivity, provide excellent stability and convective heat transfer coefficients, and only slightly increase the pressure drop and required pumping power [6]. Many studies have been conducted to enhance the thermal properties of heat transfer fluids by adding highly thermally conductive nanoparticles [7]. Recently, a significant number of studies have been performed on carbon-based nanostructures [8], including carbon fiber [9], carbon black [10], carbon nanotubes (CNTs) [11], graphite [12], graphene oxide (GO) [13], graphene [14], and graphite flakes [15].

An experimental investigation of the convective heat transfer coefficient for nanofluids flowing through different types of tubes has been conducted in several studies [16], and these have considered different types of nanoparticles, including oxides, nitrides, metals, diamond, and carbon-based nanoparticles [17,18]. Early

* Corresponding authors. Tel.: +60 3 7967 4582; fax: +60 3 7967 5317.
E-mail addresses: mohamad.mehrali@siswa.um.edu.my, mehrali.gary@gmail.com (M. Mehrali), salimnewaz@um.edu.my (S.N. Kazi).

http://dx.doi.org/10.1016/j.ijheatmasstransfer.2014.10.006
0017-9310/© 2014 Elsevier Ltd. All rights reserved.

Nomenclature

C_p	specific heat capacity, J/kg K
$C_{1\varepsilon}$, $C_{2\varepsilon}$, $C_{3\varepsilon}$, σ_k, σ_ε	model constants
D	tube diameter, m
DW	distilled water
f	friction factor
G_b	generation of turbulence kinetic energy
h	convective heat transfer coefficient
I	electrical current, A
k	thermal conductivity, W/m K
L	tube length, m
Nu	Nusselt number
P	heater power, W
Pr	Prandtl number
q''	heat flux, W/m^2
Re	Reynolds number
T	temperature, K
V	volts, V
U	mean velocity, m/s
w	water
wt%	weight percentage
X, Y, Z	Cartesian coordinates

Greek

μ	dynamic viscosity, Pa s
μ_t	turbulent viscosity
ε	turbulent dissipation
ρ	density, kg/m^3
η	thermal performance factor

Subscripts

avg	average
b	bulk
bf	base fluid
i	inner
in	inlet
m	mean
nf	nanofluid
np	nanoparticle
o	outer
out	outlet
w	wall

experiments with TiO_2, Al_2O_3, and SiO_2 nanofluids were undertaken by different researchers to determine the effect of the nanofluid concentration on the thermo-physical properties and the heat transfer coefficient [19,20]. They observed an increase in the convective heat transfer coefficients at various concentrations of the nanofluid under laminar and turbulent flow conditions from 20% to 350% [20,21]. They concluded that the influence of the nanofluid concentration on the heat transfer coefficient is significant in the turbulent region versus the laminar region [22,23]. However, only limited research has been performed on convective heat transfer when using carbon-based nanofluids as the heat transfer liquid compared with many results for the thermo-physical properties of nanofluids [22].

Numerical modeling of convective heat transfer of nanofluids can be conducted using single-phase or multi-phase approaches. Most of the studies in this area have been made using single-phase model [24–26]. The numerical and experimental works on the effective thermal conductivity and convective heat transfer are needed to demonstrate the full potential of nanofluids [27] and to understand the fundamentals of heat transfer for developing new nanofluid. Although there are recent developments in the theoretical and experimental results to understanding of the particle movements mechanisms, heat transfer and fluid flow behavior of nanofluids [27]. Many research works are available on the numerical study of convective heat transfer of nanofluids, there is no complete research on various effective parameters in this area, including based fluid, nanoparticle shape, and type of nanoparticles. However, improvement in heat transfer performance due to the nanofluids is accompanied by a number of undesired effects, including pressure drop and pumping power. Hence, it requires to obtain the proper nanofluid for optimum operation of heat transfer applications [28].

The aqueous suspensions of stable homogeneous GNP nanofluids were prepared by high-power ultrasonication. The stability and the thermo-physical properties of the GNPs have been reported previously by Mehrali et al. [1]. The main scope of the present study is to identify the uncertainties in experimental and theoretical formulations due to the effects of aqueous GNP (specific surface areas of 500 m^2/g) nanofluid on surface temperature and Nusselt number. The effects on the convective heat transfer that is derived from the different heat fluxes (8231, 10,351, 12,320 W/m^2) of the GNP nanofluid at different concentrations (0.25, 0.05, 0.075, and 0.1 wt%) under different Reynolds number varied from 4583 to 18,187.

2. Description of the experiment

2.1. Experimental system

The experimental setup for this work is shown in Fig. 1. It consists of a flow loop (with a bypass), a heating unit, a cooling part, measuring instruments, and a control unit. The flow loop includes a pump, a magnetic flow meter, a reservoir tank, a differential pressure transmitter, and a test section. The nanofluids were pumped from a 14-L capacity stainless steel jacketed tank by a Cole-Parmer magnetic drive pump at a flow rate of 0–10 l/m, and the pump flow was controlled by a Hoffman Muller inverter. The flow rate and the pressure loss were measured using a magnetic flow meter and a differential pressure transmitter, respectively. A straight stainless steel tube with a length of 1400 mm, a 12 ± 0.2-mm outer diameter, and a 10-mm inner diameter was used as the test section. The test section was heated using an ultra-high-temperature heating tape (Omega, USA) at a maximum power of 900 W, which was linked to a Variac transformer and a watt/amp meter. Five type K thermocouples (Omega, Singapore) were fixed using a high-temperature epoxy glue at equal axial distances on the outer surface of the test tube (Fig. 2).

To measure the cold and hot nanofluid temperatures, two RTD (PT-100) sensors (Omega, Singapore) were inserted to measure the bulk temperature at the inlet and outlet of the test section. All thermocouples and RTDs were calibrated against an Ametek temperature calibrator (AMETEK Test & Calibration Instruments, Denmark). The thermocouples were connected to the Graphtec (midi logger gl220), and the RTDs were connected to the Scada system for the continuous monitoring and recording of the temperature data by a personal computer. To minimize the heat loss to the surroundings, a thick glass wool wrapping was used. This insulation's heat loss temperature was measured by three type K thermocouples that were located on the outer surface of the insulation.

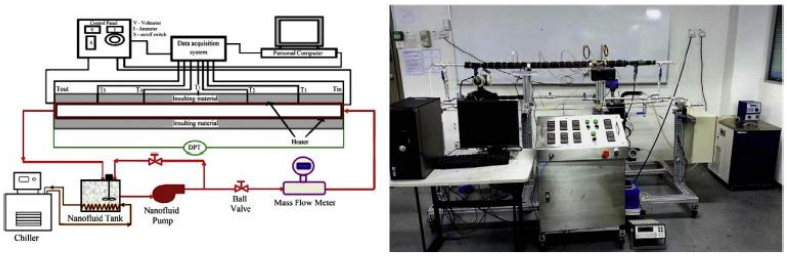

Fig. 1. Experimental setup for the measurement of the convective heat transfer coefficient.

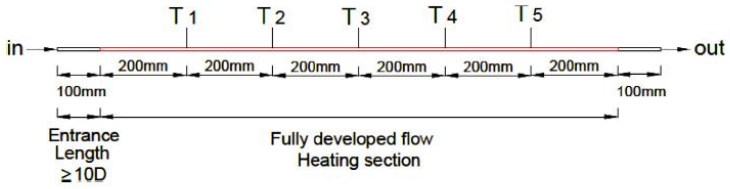

Fig. 2. Sectional view of the experimental test sections.

Table 1
Specifications and errors for the measuring devices utilized in the present experiment.

Measured parameter	Type	Range	Error
Surface temperature	Type K thermocouple	0–300 °C	±0.1 °C
Bulk Temperature	RTD (PT-100) sensor	0–200 °C	±0.1 °C
Fluid flow rate	Schmierer, Electromagnetic Flow Meter	0.1–10 m/s	±0.5%
Fluid pressure drop	ALIADP, Differential Pressure Transmitter (DPT)	0–25 kPa	±0.075%
Cooling unit	WiseCircu, DAIHAN Scientific, Refrigerated circulating bath	2.2 kW	±0.1 °C

The specifications and the accuracy of the measuring equipment used in the present experimental setup are presented in Table 1.

3. Numerical simulation

3.1. Description of the configuration

An investigation of the heat transfer behavior of the nanofluids was performed by evaluating the Nusselt number and the surface temperature. The measurements were performed in Reynolds number range varied from 4583 to 18,187 and heat flux varied from 8231 W/m^2 to 12,320 W/m^2, the weight percentage of GNP nanoparticle varied between 0.025 wt% and 0.1 wt%. A single-phase model adopted here to describe the turbulent heat transfer of the graphene nanoplatelets nanofluids in a horizontal stainless steel tube that was subjected to a uniform heat flux at its outer surface and constant fluid inlet temperature of 303.15 K, as shown in Fig. 3.

3.2. Governing equations

Continuity, momentum and energy equations in three dimensions are used for incompressible fluid. According to control volume method based on converting the governing equations to algebraic equations of Herrmann [29,30] that is defined below:

$$\frac{\partial U_i}{\partial x_i} = 0 \tag{1}$$

$$\frac{\partial (U_i U_j)}{\partial x_j} = -\frac{\partial p}{\partial x_i} + \frac{\partial}{\partial x_j}\left(\mu \frac{\partial U_i}{\partial x_j} - \overline{\rho u_i u_j}\right) \tag{2}$$

$$\frac{\partial (U_i T_j)}{\partial x_j} = -\frac{\partial}{\partial x_i}\left(\frac{\mu}{\mathrm{Pr}} \frac{\partial T_i}{\partial x_j} - \overline{\rho u_i t_j}\right) \tag{3}$$

The Reynolds stresses and heat fluxes are, respectively, given as:

$$\overline{\rho u_i u_j} = -\mu_t \left(\frac{\partial U_i}{\partial x_j} + \frac{\partial U_j}{\partial x_i}\right) + \frac{2}{3}\delta_{ij} k \tag{4}$$

$$\overline{\rho u_i t_j} = -\frac{\mu_t}{\sigma_\theta} \frac{\partial T_i}{\partial x_j} \tag{5}$$

The standard k–ε model has two transport equations for the turbulence kinetic energy and energy dissipation that are solved together with the equations of balance by the finite volume method Launder [31,32]. The corresponding transport equations given below:

$$\frac{\partial \rho k U_i}{\partial x_j} = -\frac{\partial}{\partial x_j} + \left[\left(\mu + \frac{\mu_t}{\sigma_k}\right)\frac{\partial k}{\partial x_j}\right] + \rho(G_b - \varepsilon) \tag{6}$$

$$\frac{\partial \rho \varepsilon U_i}{\partial x_j} = -\frac{\partial}{\partial x_j} + \left[\left(\mu + \frac{\mu_t}{\sigma_k}\right)\frac{\partial \varepsilon}{\partial x_j}\right] + \rho \frac{\varepsilon}{k}(C_{1\varepsilon} G_b - C_{2\varepsilon}\varepsilon) \tag{7}$$

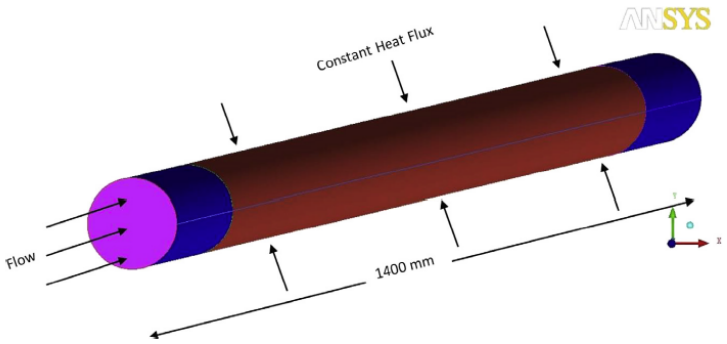

Fig. 3. 3D view of the test sections.

$$G_b = \mu_t \left(\frac{\partial u_i}{\partial x_j} + \frac{\partial u_j}{\partial x_i} \right) \frac{\partial u_i}{\partial x_j} \tag{8}$$

$$\mu_t = \rho c_\mu \frac{k^2}{\varepsilon} \tag{9}$$

The standard constants used in the k–ε model are $C_{1\varepsilon} = 1.44$, $C_{2\varepsilon} = 1.92$, $C_{3\varepsilon}$, $\sigma_k = 1.0$, and $\sigma_\varepsilon = 1.3$.

3.3. Numerical procedure

ANSYS ICEM software was used to create the geometry and meshing was illustrated in Fig. 4. The governing equations were solved by computational fluid dynamic software ANSYS FLUENT 14 based on associated boundary and initial conditions. According to [33] the finite volume method was applied to discretize the governing equations in the computational domain. The SIMPLE algorithm coupling for velocity and pressure [34,35], a second order upwind scheme for discretization of all equations were considered. Non-uniform quadrilateral grids were used for meshing the solution domain. In order to obtain high accuracy data, the residual sum was computed and set for each iteration and the convergence criterion was less than 10^{-6} for all equations.

3.4. Grid independence

In order to evaluate the grid independent results four sizes of grid were adopted for DW at Reynolds number of 18,187 and uniform heat flux of 12,320 W/m^2 with different dimensional units of x, y, z, as shown in Table 2. The second grid is represents the grid independence due to the difference in average Nusselt number between the second and fourth grid was less than 0.7%.

4. Materials, nanofluid preparation and stability measurements

To investigate the effect of the nanoparticles on heat transfer and thermal performance, the GNP nanofluid was prepared by using a two-step method without any surfactant. As described in our previous work [1], GNPs (Grade C, XG Sciences, Inc., Lansing, MI, USA) were used for the preparation of nanofluids. The specifications of the GNP nanoparticle are shown in Table 3. The GNPs were dispersed in distilled water using a high-powered ultrasonication probe (Sonics Vibra-Cell, VC 750, Sonics & Materials, Inc., USA) with a 750-W output power and a 20-kHz frequency power supply. The concentrations of the nanofluids were 0.025, 0.05, 0.075, and 0.1 wt%.

According to our previous work on stability and characterization of GNP nanofluid [1], the GNP show good flexibility as proved by the folded and/or rolled parts. This indicates that each of the GNP sheets only contains a very limited number of graphene layers, which is consistent with the parameter provided by the manufacturer [1,36]. Additionally, Mehrali et al. [1] reported that the colloidal stability of the GNP nanofluids for the concentrations of 0.025, 0.05, 0.075 and 0.1 wt% remains relatively constant after 600 h and only reduced by 4.8%, 8.1%, 8.4% and 12.3%, respectively. Although the amount of reduction was different for each nanofluid, the reductions were comparatively low in all concentrations, which agree well with the results of the previous studies [1].

The UV–vis spectrophotometer analysis and zeta-potential measurements are a convenient approach to characterize the stability of nanofluids (Fig. 4). The stability of GNP nanofluids under UV-vis indicated that the nanofluids were stable upto 30 days with maximum sedimentation of 14% for 0.1 wt%. Therefore, the suspension stability of the prepared nanofluids verified by measuring periodically reflective index (absorption) from UV–vis spectropho-

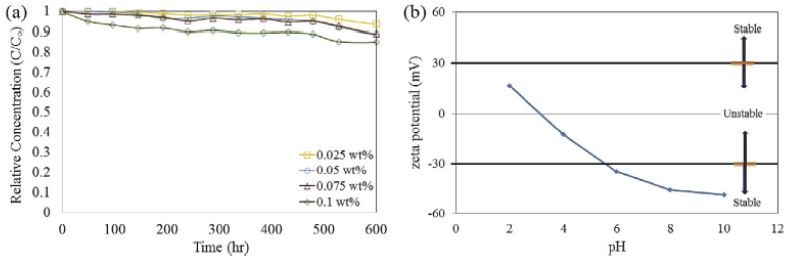

Fig. 4. (a) Relative particle concentration of nanofluids with sediment time, (b) zeta potential values of GNP nanofluids as a function of pH value.

Table 2
Grid independent for pure water at q = 12,320 W/m^2 and 1.3 m/s.

Size of grid	$X = 15, Y = 15, Z = 600$	$X = 20, Y = 20, Z = 1200$	$X = 25, Y = 25, Z = 1500$	$X = 30, Y = 30, Z = 1800$
Grid no.	1	2	3	4
Nu_{ave}	123.5541751	123.9607365	124.1866204	124.9396083

Table 3
GNP nanoparticle specifications.

Property	Specification
Particle	Graphene nanoplatelets (GNPs)
Color	Black granules/powder
Carbon content	>99.5
Bulk density	0.2–0.4 g/cm^3
Relative gravity	2.0–2.25 g/cm^3
Specific surface area	500 m^2/g
Particle diameter	2 μm
Thickness	2 nm
Thermal conductivity (parallel to surface)	3000 W/m K
Thermal conductivity (perpendicular to surface)	6 W/m K

tometer of the stationary nanofluid maintained at 30 °C. In the other hand, zeta potential value of −37.8 mV for the natural pH suggested that the stability of GNP nanofluids were acceptable for heat transfer applications.

Fig. 5 shows a visual inspection of GNP nanofluids after heat transfer run while there was no sedimentation and agglomeration in the GNP nanofluids. These results indicate that the GNP nanofluids were stable even after the heat transfer run.

The TEM image (Fig. 6(a)) of the GNP nanofluids indicated that the GNP sheets only contains a very limited number of graphene layers, which is consistent with the parameter provided by the manufacturer. The SEM image (Fig. 6(b)) shows that the GNP nanofluid with concentration of 0.1 wt% has no aggregation and well dispersed.

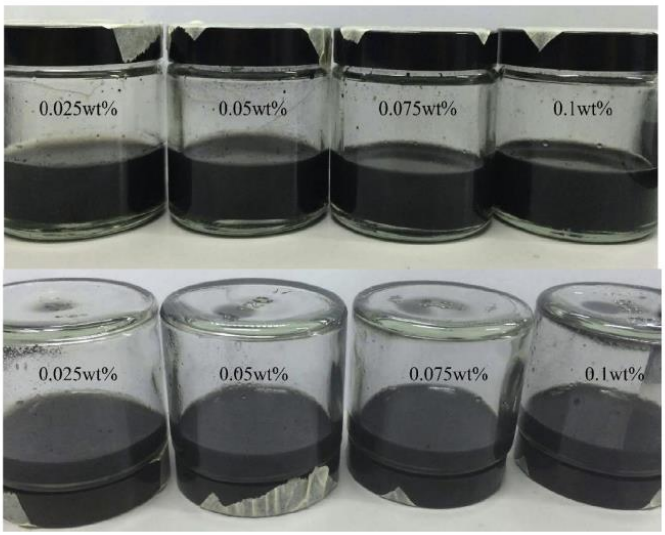

Fig. 5. Visual investigation of sedimentation of nanofluids after heat transfer run.

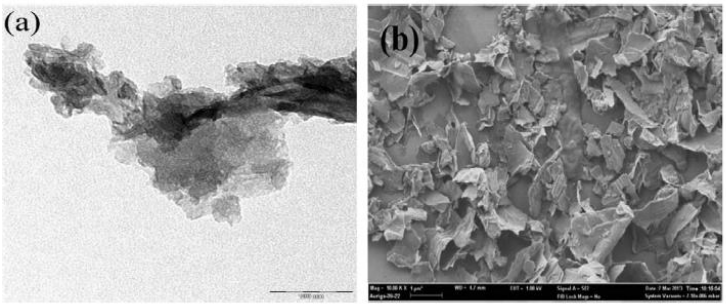

Fig. 6. (a) TEM (b) SEM image of the GNPs.

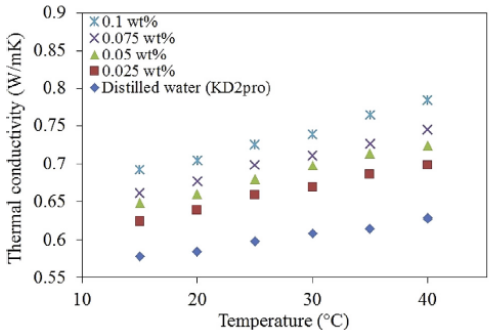

Fig. 7. Effects of temperature and concentration on the thermal conductivity of GNP nanofluids.

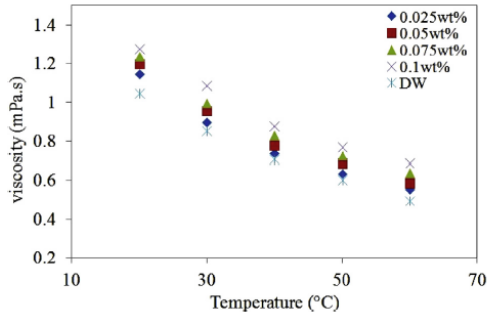

Fig. 8. Viscosity of the GNP nanofluids as a function of temperature.

4.1. Measurement of the effective thermal conductivity and the viscosity of the nanofluids

The thermal conductivity is measured by using a KD2 Pro thermal analyzer (KD2 Pro, Decagon Devices, Inc., Pullman, WA, USA), which works on the principle of a transient hot wire method with a 2–4% accuracy. Fig. 7 shows the effective thermal conductivity of the GNP nanofluids as a function of the temperature at different concentrations. The effective thermal conductivity increases as the nanofluid temperature increases in each case, and a linear dependence of the thermal conductivity enhancement on the temperature was obtained. The enhancement of thermal conductivity for GNPs 500 was between 7.96% and 25%.

The viscosity of the GNP nanofluids at a different weight percentage was measured by using an Anton Paar rheometer (Physica MCR 301, Anton Paar GmbH, Graz, Austria) at different temperatures with a 1% error rate. The viscosity of the nanofluids is one of the most critical parameters determining the quality of the heat transfer fluid. Similar to the simple fluids, temperature is the main parameter affecting the viscosity of the nanofluids. Fig. 8 shows the viscosity at a high shear rate of 500 s^{-1} for different concentrations as a function of temperature. It can be seen that viscosity reduced with the raising of temperature and decreased between 9% and 38%. The loading of the GNP nanoparticles increase the friction and flowing resistance of fluids that ultimately causes increase of viscosity. Moreover, by rising the temperature, the nanoparticles are motivated more and create a more space for them. This is expected due to the weakening of the inter-particle and inter-molecular adhesion forces and similar trends are been observed for almost all other varieties of nanofluids.

5. Results and discussion

5.1. Validation of the numerical method for the case of distilled water

The numerical results for DW at constant heat flux conditions were compared with the experimental results of DW. Fig. 9 shows that the comparison between the experimental tube surface temperature and the data from the numerical simulation for Reynolds number of 4583 and 18,187 at different heat flux. It can be seen that linear increases in surface temperature along the pipe and those increment occurred with increase of Reynolds number and heat fluxes for both experimental and numerical results. There is a good agreements between numerical and experimental data with an error of less than 2% for DW.

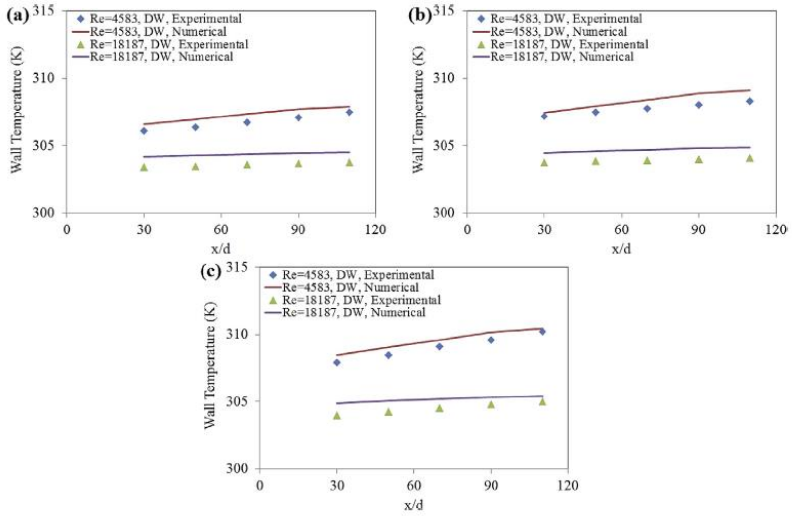

Fig. 9. Measured surface temperature and the numerical data for distilled water versus the non-dimensional axial distance (x/d) at a different heat flux; (a) 8231 W/m^2, (b) 10,351 W/m^2, (c) 12,320 W/m^2.

5.2. Heat loss calculation

The heat transfer coefficients were calculated based on the measured values for the inlet, outlet, and inner wall temperatures and the flow rate. From the insulation surface temperatures, convective and radioactive heat loss to the surroundings were evaluated and found negligible. The heat loss can be calculated by the Eq. (10) and Fig. 10 shows that the deviation was lower than 9.7% under the conditions of this work:

$$Heat\ loss = \dot{q}_{Num} - \dot{q}_{exp} \tag{10}$$

5.3. Validation test for distilled water with different classical correlation

To validate the reliability of the experimental setup for calculating the Nusselt number and for providing a baseline to compare the GNP nanofluid data, tests were initially conducted for distilled water (DW). The experimental results for DW at constant heat flux conditions were compared with the results from the standard equations, such as the Gnielinski, Petukhov, and Dittus–Boelter equations for turbulent flow [37]. Fig. 11 shows a comparison between the experimental average Nusselt number and the data from the above mentioned equations. The experimental data and classical correlations agree well. Data from the Petukhov equation and the experimental Nusselt number for distilled water are better than the data from the other equations and validate the accuracy of the experimental setup with an error rate of less than 6%.

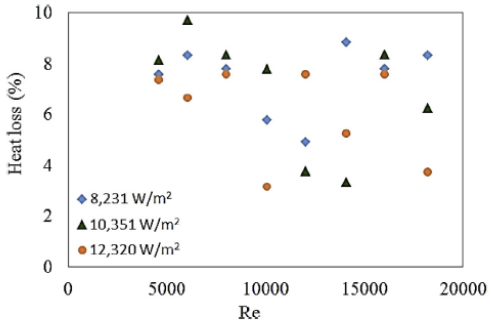

Fig. 10. Heat loss calculation.

5.4. Uncertainty analysis of the test results

The uncertainty analysis of the measured data along with that of the relevant parameters obtained from the data reduction process is presented in Table 4 and is estimated based on the error propagation method [38,39].

5.5. Comparison between numerical and experimental results of GNP nanofluid

Fig. 12 shows the numerical and experimental inner wall surface temperature at different axial distance for GNP nanofluid at Reynolds number of 4583 and 18,187. It was observed that the surface temperature increases when the heat flux increase and that depends on GNP concentration. Inner wall temperature distribution results are compared with the experimental results and were found with error of 4% for GNP nanofluid. Similarly, the local convective heat transfer coefficient and the Nusselt number along the tube were obtained from the Newton's cooling law.

As seen in Fig. 12, the temperatures significantly decreased on increases of the particle concentration. Experimental and numerical results shown that the using of the GNP nanofluid has better heat transfer characteristics than the using of DW. As Reynolds number increases, the deviation between the numerical and experimental wall temperature become less and at higher Reynolds number has revers effect. This effect is due to the fact that the corresponding velocity profiles become more uniform as Reynolds number increases [40].

As shown in Fig. 12, in the fully developed region and in the case of constant heat flux, the surface temperature will increase linearly in the flow direction. Previous studies claimed that the

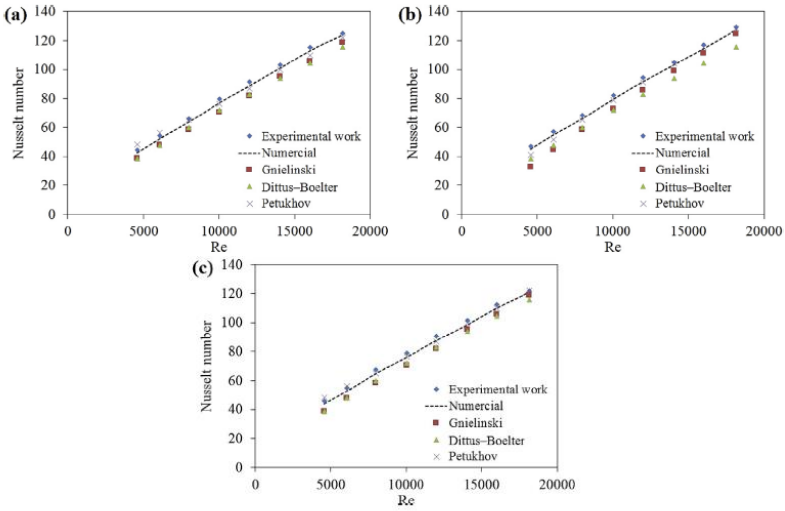

Fig. 11. Measured average Nusselt number and the prediction correlations for distilled water versus the Reynolds at a different heat flux; (a) 8231 W/m^2, (b) 10,351 W/m^2, (c) 12,320 W/m^2.

Table 4
Uncertainty ranges.

Variable name	Uncertainty range (%)
Nu, *avg*	±6
Nu, *Local*	±8
h, *avg*	±6
h, *local*	±9
f	±10

reasons for the heat transfer enhancement of the nanofluids included the mixing effects of the particles near the wall, particle migration, particle shape and re-arrangement, the Brownian motion of the particles, the thermal conductivity enhancement, a reduction of the boundary layer thickness, and a delay in the boundary layer development [41,42]. In addition, the thermal entry length for a fully developed flow in the turbulent region should be expressed as $x \geqslant 10D_i$ [21,43]. According to the experimental findings, there are two reasons for the convective heat transfer enhancement of the nanofluids: delay and disturbance of the thermal boundary layers and the excellent thermal conductivity enhancement of the GNP nanofluid. The chaotic movements created from the Brownian motion and the migration of GNP nanoparticles could affect the development of the thermal boundary layer in the entrance region [41].

Fig. S1 shows the results counter of inner wall surface temperature for the GNP nanofluid at different Reynolds number, 0.1 wt% and 12,320 W/m^2 heat flux. It can be seen that the tube wall temperature was change by increasing of Reynolds number.

5.6. Comparison of the Nusselt number

Average Nusselt numbers of the GNP nanofluids as a function of the Reynolds number at different heat fluxes are presented in Fig. 13. Generally, for all cases the average Nusselt numbers of the GNP nanofluids observed good increment with increase of Reynolds number in both numerical and experimental results. Effect of weight concentrations of the GNP nanofluids on average Nusselt numbers has been noted where the highest average Nusselt number showed at 0.1 wt%, Re = 18,187 and heat flux of 12,320 W/m^2 due to the improved thermal conductivity and the reduced thermal resistance between the flowing nanofluid and the inner wall surface of the tube. The Nusselt number (Nu) was increased up to 75%, 79%, and 83% for the heat fluxes of 8231, 10,351, and 12,320 W/m^2, respectively.

5.7. Pressure drop of the nanofluid

To use the nanofluids in practical applications, the flow features of the GNP nanofluids should be determined in addition to the heat transfer measurements. The experimental results show that the pressure drop and the friction factor depend on the GNP concentration and Reynolds number (Fig. 14). Table 5 shows the pressure

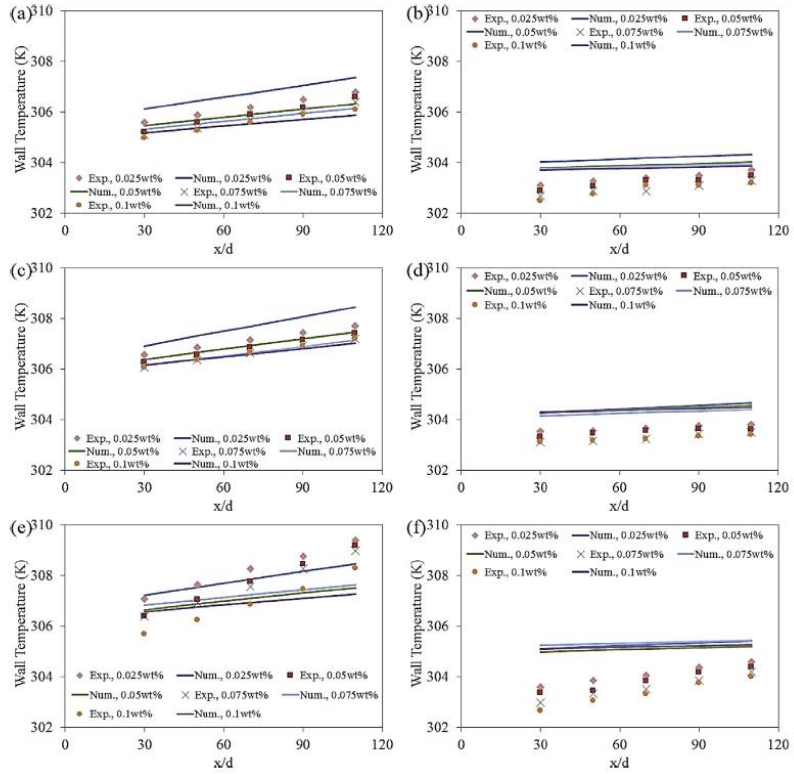

Fig. 12. Distribution of inner wall temperatures of tube surface for different heat flux and Reynolds; (a) 8231 W/m^2, Re = 4583, (b) 8231 W/m^2, Re = 18,187, (c) 10,351 W/m^2, Re = 4583, (d) 10,351 W/m^2, Re = 18,187, (e) 12,320 W/m^2, Re = 4,583, (f) 12,320 W/m^2, Re = 18,187.

Link to Full-Text Articles :

http://www.sciencedirect.com/science/article/pii/S0017931014008916

www.researchgate.net/profile/Hussein_Togun2/publication/267506318_An_experimental_and_numerical_investigation_of_heat_transfer_enhancement_for_graphene_nanoplatelets_nanofluids_in_turbulent_flow_conditions/links/5450da640cf201441e94d4a5.pdf